

# We are IntechOpen, the world's leading publisher of Open Access books Built by scientists, for scientists

4,800

Open access books available

122,000

International authors and editors

135M

Downloads

Our authors are among the

154

Countries delivered to

TOP 1%

most cited scientists

12.2%

Contributors from top 500 universities



WEB OF SCIENCE™

Selection of our books indexed in the Book Citation Index  
in Web of Science™ Core Collection (BKCI)

Interested in publishing with us?  
Contact [book.department@intechopen.com](mailto:book.department@intechopen.com)

Numbers displayed above are based on latest data collected.  
For more information visit [www.intechopen.com](http://www.intechopen.com)



# Introductory Chapter: Growing W Single Crystals by EBFZM for Studying Mechanical Behavior

*Vadim Glebovsky*

## 1. Introduction

Tungsten (W) is one of the most perspective metals for different applications of its physical and chemical properties [1]. An incredible complex of diversified natural properties, such as mechanical properties, wear, and radiation resistance, stimulates a wide use of high-purity W single crystals in many modern applications, sometimes like quite unexpected ones, that is, W single crystals as high-resolution STM tips or elements of sputter composite magnetron targets for very-large-scale integration (VLSI) metallization [2, 3].

Electron-beam floating zone melting technique (EBFZM) is a unique technique for the crucibleless melting of such refractory metals as W, when it is contraindicated to have any contact with any refractory materials. This method is practically indispensable for the melting, refining, and growing of tungsten single crystals. As a result of numerous studies, it was established that the structure of tungsten crystals under the influence of large temperature gradients can differ from ideal. The author and his colleagues dealt with this structural problem for a long time. Single crystals of BCC refractory metals grown from the melt contain a lot of dislocations, so their density in regular samples can be up to  $10^5$  to  $10^7$   $\text{cm}^{-2}$ . In many studies, it is shown that most of these dislocations aggregate into walls and grids, thus forming a characteristic dislocation substructure [4–6]. This chapter presents the results of the complex studies of the growth and mechanical properties of W single crystal by EBFZM depending on the growth rate, seed perfection, and axial temperature gradients. It seems that single crystals of W are the optimal objects for studying both growth processes and plastic deformation processes. I am confident that the studies presented in this chapter will contribute to further progress in this area. For several years, studies have been conducted in which attempts have been made to find out what prevents the growth of more or less perfect single crystals of W, on the one hand, and, on the other hand, attempts have been made to understand the patterns of plastic deformation of W over a wide temperature range.

Because single crystals of high-purity metals like W, Mo, Ta, and Nb, grown from the melt have the dislocation structure, characterized by blocks and boundaries thus, in our opinion, it is more correct to use such words as substructure, sub-blocks, or sub-boundaries. Several mechanisms for the appearance of dislocations and, accordingly, a characteristic substructure in the process of growing crystals are experimentally investigated before studying the mechanical behavior of W single crystals: under the action of the thermal gradients and mechanical stresses developed at the crystal growth, other factors have no such pronounced influence.

An investigation of the impact of a number of technological parameters of EBFZM on the substructure of grown single crystals has been carried out on the newly created growth equipment using fundamentally new electron guns allowing

growing crystals of the optimal length and diameter in fully reproducible temperature conditions. The new electron gun is designed to form a stable circular electron beam. The main advantages of the gun are practically complete absence of a condensate of the melted metal on the circular cathode, fine focus of the circular electron beam on the crystal (anode) due to the focusing electrode system, the ability to grow crystals of different diameters through the use of a set of replaceable focusing electrodes, the stability and reproducibility of the temperature profile on the growing crystal, and an absence of warped elements in the design of the EB gun in the process of long-term work due to its fabrication of a water-cooled copper.

Nevertheless, the seed, growth rate, interstitials, and temperature profile on an interface have a significant effect on the final structural quality of grown crystals. In our studies, the chemical composition and temperature profile are kept constant due to the use of the original EB gun and pre-refined blanks, so it is always possible to distinguish the effect of the growing rate in a pure form. The role of the growth rate is of high importance in both the crystallization stage and cooling to room temperature (RT), starting beyond the interface between the liquid metal and the crystal. In bulk BCC metals, grown from the melt, deformation at RT is a rule controlled by dislocations with higher lattice resistance. Nevertheless, I am absolutely convinced that such a metal as W, which possesses such a unique complex of excellent properties, should be investigated, despite the enormous difficulties that must be overcome.

## 2. Growth of W single crystals and study of their plasticity

### 2.1 Introduction

The crucibleless melting methods are especially important in the production and investigation of single-crystalline W of high purity, since this metal has a high melting point and is chemically active in the liquid state. Along with cylindrical W single crystals, much attention is paid to W bicrystals, which are an extremely interesting object in carrying out various kinds of materials science studies, since it allows one to study grain boundaries with given crystallographic parameters. Although the structure of W single crystals has previously received quite a lot of attention, many questions arise as to the possibilities of improving the structural quality of W crystals, which requires a detailed analysis of factors that have a decisive influence on the formation of the structure. This explains the great interest to studies of ways to improve the structural quality of W single crystals depending on the growth parameters, namely, the rate of crystallization, electron beam intensity fluctuations, and the crystallographic perfection of seeds.

In conformity with the experimental results of dynamic tensile measurements, a form of the hardening curves depends on an orientation of a tensile axis of the specimens. For the orientation of the tensile axis near  $\{1\ 1\ 0\}$ , the stress-strain curves give an information on following small work-hardening, whereas for other tensile axes, a significant work-hardening after the elastic limit is discovered. As to glide systems, the  $\{1\ 1\ 0\}$   $[1\ 1\ 1]$  glide system at low-temperature regime is operative, while at RT and above  $\{1\ 1\ 2\}$  slip planes also appear. In this chapter, dynamic tensile measurements on W monocrystalline specimens at  $T$  from 25 to 800 K are presented. The crystal axis orientation of tensile specimens has been chosen at the middle of the stereographic triangle because such a choice allows one to obtain the greatest stress in a  $\{1\ 1\ 0\}$   $[1\ 1\ 1]$  slip system. As known, BCC metals at plastic deformation go through a ductile-to-brittle transition. The flow stress also strongly depends on  $T$ . The brittle behavior is noted in the cleavage form predominantly on the planes  $\{1\ 1\ 0\}$  and  $\{1\ 0\ 0\}$ .

## 2.2 Growth of W single crystals

Zone purifying of the starting material and growth of single crystals is carried out in a vacuum of  $10^{-5}$  to  $10^{-7}$  Torr at a power up to 25 kW, voltage up to 20 kV and cathode heating current up to 40 A. In accordance with the design capabilities of the setup, the diameter of W single crystals can be correctly varied from 4 to 30 mm. For effective melting and growing of single crystals, a fundamentally original electron gun has been developed (**Figure 1**). In fact, the electron gun is an electrostatic lens and provides rotation and focus of the annular electron beam. The gun is very reliable—the duration of continuous operation covers the most stringent technological requirements associated with refining an initial metal and growing single crystals. With the help of the original electron gun, it is possible to carry out long vacuum purifying and growing single crystals of W of any geometry, which is practically impossible when using the known guns.

During the EB zone vacuum melting, a deep purification of the liquid W occurs due to evaporation of volatile metallic and nonmetallic impurities. Thanks to this, it is possible to obtain W crystals with a very low content of impurities, often beyond the limits of detection by modern analytical methods (mass spectrometry with inductively coupled plasma, fast neutron activation, etc.). The stage of diffusion transparency of a liquid metal, when impurities diffuse extremely fast from the volume to the surface of the melt, is realized most effectively in the process of EBFZM in vacuum due to the phase transition of a metal from a solid state to a liquid one.

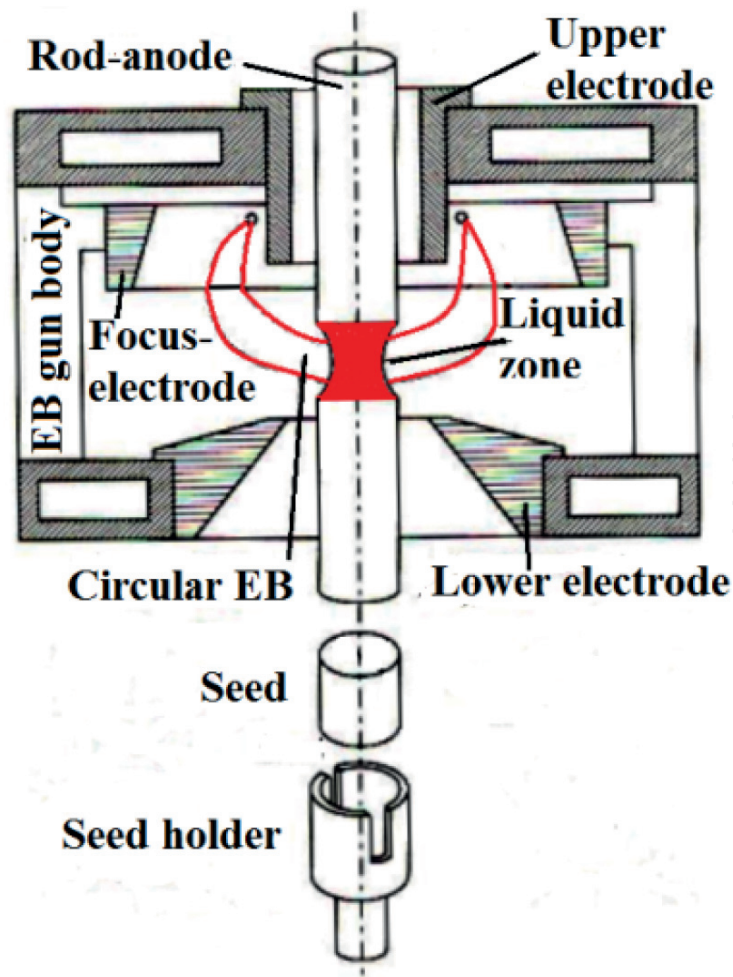


**Figure 1.**  
*A cathode unit (EB gun) for the EBFZM growth of W single crystals.*



For this study, W single crystals having growth axes [1 1 0], [1 0 0], and [1 1 1] are of a diameter of 10 mm. The crystallographic orientations of both the seeds and growth axes are checked by Laue X-ray diffraction. Structural studies are done with both electron and optical microscopies. It is shown that all specimens are single crystals of the high quality, and their dislocation density is of  $5 \times 10^5 \text{ cm}^{-2}$ . The substructure has been also studied by the angular scanning X-ray topography which determined the position, size, and misorientation angles of subgrains. This technique consists in mapping an intensity of the diffracted beam over the crystal cross section in a fixed Bragg geometry. Samples after erosion cutting and mechanical grinding are subjected to electrolytic polishing and etching. The residual resistivity ratio demonstrates an integral purity of specimens and is measured by a four-contact technique. All W specimens used in our study have  $R_{300\text{K}}/R_{4.2\text{K}} = 70,000$ . A typical chemical composition of high-purity refractory metals studied is given in Refs. [3–5]. Since the fulfillment of the tasks posed to a large extent depends on the structural quality of the crystals, the presence of the growth equipment for growing crystals with fully reproducible growth parameters is of great importance. It is already noted earlier that crystals of refractory metals have a characteristic dislocation structure with a subgrain size, which can be conditionally divided into three orders (**Table 1**). The structural quality of grown single crystals depends on the growth rate, thermal stresses, interstitials, inheritance of the seed structure, and supersaturation of the lattice with vacancies. The growth rate or travel of the liquid zone is one of the basic parameters. At a high temperature, dislocations, regardless of their nature, are very mobile, as a result of which the dislocation structure is polygonized. Along with the increased mobility of dislocations, a considerable contribution to the formation of a polygonized structure is also contributed by mechanical stresses. The growth rate of the crystals is from 0.2 to 50  $\text{mm min}^{-1}$ . Usually, three passes of the liquid zone are necessary to get a crystal of both the high chemical purity and structural quality: N1 pass at 6  $\text{mm min}^{-1}$ , N2 pass at 2  $\text{mm min}^{-1}$ , and N3 pass at a given rate from the above interval. N1 and N2 passes are refining ones, and N3 pass is intended for growing a single crystal on a seed.

The structure of W crystals is somewhat different depending on the rate of the crystal growth. Crystals grown at a low rate ( $0.5 \text{ mm min}^{-1}$ ) are characterized by a developed substructure, with an average subgrain belonging to the second order (**Table 1**). The average subgrain size reaches 100  $\mu\text{m}$ ; the dislocation density calculated from the etch pits is of  $3 \times 10^5 \text{ cm}^{-2}$ . At a high growth rate ( $6 \text{ mm min}^{-1}$ ) the substructure contains separate etch pits without polygonal boundaries. The dislocation density is  $\sim 1 \times 10^6 \text{ cm}^{-2}$ . Another structural feature of W crystals grown at all rates is an inhomogeneity of the microstructure in the radial direction. The central part of a crystal is free of the subboundaries, and intensive polygonization can be observed at the periphery of the specimen. The block structure is most developed near the surface, and the boundaries of sub-blocks of the first order in the center of the crystal are absent; a misorientation angle of sub-blocks of the second order decreases

Order of substructure	Mean size of subgrains	Misorientation between subgrains
First order	1 mm < d < 8 mm	$30' < \Theta < 4^\circ$
Second order	50 $\mu\text{m}$ < d < 1 mm	$30'' < \Theta < 30'$
Third order	0 < d < 50 $\mu\text{m}$	$0 < \Theta < 30''$

**Table 1.**  
*The substructure parameters of W single crystals.*

substantially and the sub-blocks themselves are more equiaxed. These data indicate that the growth rate completely determines the nature of the substructure of the growing crystal.

The characteristic microstructure of  $W[0\ 0\ 1]$  crystals has been revealed on the  $(0\ 1\ 0)$  plane. This plane and the growth axis are parallel. The subgrain boundaries propagate over long length along the growth axis. They are dislocation grids left by dislocations having Burgers vectors  $a/2[1\ 1\ 1]$  and  $a[1\ 0\ 0]$ , characteristic for the BCC lattice. The average subgrain size can reach  $400\ \mu\text{m}$ . The substructure of the  $W(1\ 1\ 0)$  single crystal is determined by the method of angular scanning X-ray topography. The subgrain is usually shown in various shades of gray; the light intervals correspond to the small-angle boundaries between them. Significant changes in the substructure are observed at the extra-high rates ( $>10\ \text{mm min}^{-1}$ ), when sub-boundaries appear in crystals with the misorientation angles up to  $3\text{--}5^\circ$ . It is experimentally established that the dislocation density increases with the increasing growth rate, however, not more than an order of magnitude. Thermal gradients are measured with a help of micro-optic temperature measuring as well as estimated with a digital solution of the heat equation for a stationary crystal growth stage. These estimates show that the axial gradients of  $T$  under the crystallization front in the solid phase can reach  $1500\ \text{K cm}^{-1}$ . This leads to significant thermal stresses followed by their relaxation through plastic flow and multiplication of dislocations. In other words, the temperature gradients cause high values of the dislocation density, which leads to the appearance of a characteristic dislocation substructure.

The appearance of dislocations having Burgers vectors  $a/2[1\ 1\ 1]$  and  $a[1\ 0\ 0]$  is very probable ( $a$  is a period of the BCC). It is precisely from these dislocations arising in the growing process of the crystal, due to high thermal stresses, that small-angle boundaries form in the  $W$  single crystals a characteristic dislocation substructure. At low dislocation densities of  $10^5$  to  $10^6\ \text{cm}^{-2}$ , small-angle screw or tilt boundaries are formed; however, they consist of several dislocation systems. The fine dislocation structure has been studied on the  $W$  single crystals subjected to a high-temperature creep. The small-angle boundaries have misorientation angles of  $2\text{--}4^\circ$ , and the dislocations are resulted of plastic deformation during cooling. In BCC lattices, symmetric tilt boundaries which consist of parallel edge dislocations are most likely in  $\{1\ 1\ 1\}$  and  $\{1\ 0\ 0\}$  planes, whereas asymmetric tilt boundaries are most likely in  $\{h\ k\ 0\}$ -type planes and pure screw boundaries in  $\{1\ 1\ 0\}$ . Thus, if a dislocation system that creates small-angle boundaries in a plane layer is allowed to move by sliding or creeping, then the system of small-angle boundaries will tend to a finite number of planar grids. Based on this, the triple junctions of small-angle boundaries can differ from  $120^\circ$ . This is confirmed by our experiments on crystals which are grown at  $>1\ \text{mm min}^{-1}$  (i.e., actually annealed). In this experiments, joints of different configurations are observed on the  $\{1\ 0\ 0\}$  planes. The use of recrystallized seeds of the highest structural quality, when the dislocation density is of  $5 \times 10^4\ \text{cm}^{-2}$ , shows that boundaries germinate in a crystal. Even in the case, when the structural quality of seeds is very high, dislocations appear anew during further growing and can achieve values of  $10^6$  to  $10^7\ \text{cm}^{-2}$ . Due to polygonization the characteristic dislocation structure is formed, completely analogous to that in the regular crystals, with the misorientation angles of subgrains increasing step-by-step. The substructure of seeds is inherited by the crystals grown by EB zone melting. As a rule, boundaries presented in regular seeds also grow into a crystal. If the plane of such boundaries and the axis of a growing crystal are parallel to each other, then stable small-angle sub-boundaries persist in the crystal and sprout over long lengths. Thus, in the crystals with the growth axis  $[1\ 0\ 0]$ , there exist small-angle boundaries elongated along the growth axis and having misorientations up to  $1\text{--}2^\circ$ .

A fairly high ratio of the resistances of the investigated single crystals of W at the level of  $\sim 10^4$  to  $10^6$  indicates a high purity of the metal, which leads to an unambiguous conclusion about the insignificant role of impurities in the development of the crystal dislocation structure.

A comparison of two groups of W single-crystalline specimens has been done: as grown W crystals (AG) and strain-annealed specimens (SA). From the AG specimens, both groups of initial specimens are machined. An accuracy of the orientation of the final specimens, which depends on the structure quality, has been achieved: in the AG specimens, it is  $1^\circ$ , and in the SA specimens, it is better than  $0.1^\circ$ . To get a distinction of the structure quality of the SA and AG specimens, the characterization has been accomplished for both kinds of specimens. The AG substructures, influenced by thermal stresses, are detected after an electrolytic etching which identifies small-angle sub-boundaries separating the different subgrains. The substructure of the AG specimens W(1 0 0) contains low-angle sub-boundaries which appear as lines. An average size of subgrains is  $500 \mu\text{m}$ . The subgrains are little stretched out in the parallel to the growth axes. The etching procedure reveals point defects and dislocations. It is found that the dislocation density is of  $10^5$  to  $10^7 \text{ cm}^{-2}$ . As for the SA specimens, it is not possible to use the etching technique because small-angle boundaries are absent. Thus, for a direct comparison of the AG and SA specimens, X-ray diffraction methods are used [7]. In **Figure 2a** and **b**, rocking curves are given for the AG specimen W(1 1 0) and the SA specimen W(1 1 0). It should be noted that in **Figure 2** the AG and SA curves are with different scales: **Figure 2a** is in angular degrees, while **Figure 2b** is in angular seconds. This method is revealed in the AG specimen several subgrains of different orientations as individual peaks which indicated by arrows in **Figure 2a**. The angles between the subgrains are calculated using data for the rocking curves, and they are of about  $1^\circ$ . The structural quality of the SA specimen in comparison with the AG specimen is obvious when one compares **Figure 2a** and **b**. The rocking curve for the SA specimen does not reveal any substructure. The rocking curve across the sub-boundary is presented in **Figure 2c**. Based on the fitting of this curve and two individual curves with the width taken from the SA specimen in **Figure 2b**, it is established that the misorientation angle between two subgrains is approximately 70 arc seconds.

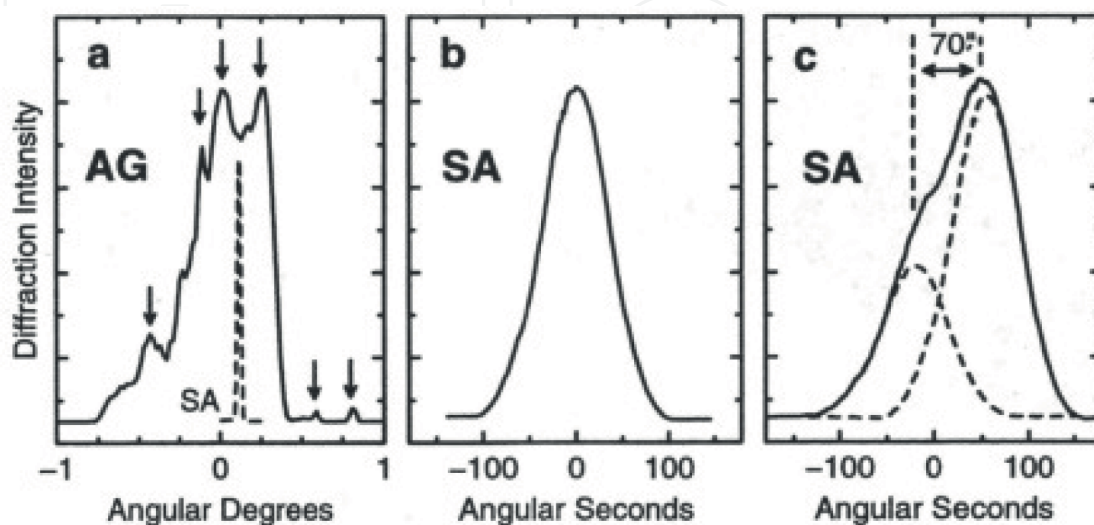


**Figure 2.** Rocking curves of W(1 1 0) specimens: (a) AS specimen, (b) SA specimen, (c) SA specimen with small-angle sub-boundary; (a) also shows the rocking curve of the SA specimen taken from (b) for comparison (dashed curve). Arrows in (a) indicate different subgrains. The rocking curve (c) is measured across small-angle sub-boundary.



### 2.3 Surface cleaning and characterization of crystals

Surface cleaning and characterization of the grown W crystals are done in the UHV setup MiniMobis ( $1 \times 10^{-10}$  mbar) [7]. To analyze an outermost atomic layer of specimens, we have used low-energy ion scattering (LEIS). These studies are performed with 5 keV  $^4\text{He}^+$  ions. Together with LEIS, two other techniques are used: Auger electron spectroscopy (AES) to analyze contaminants, having an analyzing depth of a few monolayers, and low-energy electron diffraction (LEED) to get structural data on both the specimen surface and probable superstructures on the surface. The cleaning procedures have been chosen for the SA specimen W(1 1 0) as the most characteristic case. Experimental measurements by LEIS, AES, and LEED before and after cleaning operations are presented in **Figures 3–5**. LEIS shows that W is nearly absent in the outermost atomic layer, showing that the specimen is almost completely covered with contaminants (**Figure 3**, untreated). Auger analysis also shows that C and O alone cover the surface (**Figure 4**, untreated). A significant reduction in C and O is received by sputtering the surface with 3 keV  $\text{Ar}^+$  at RT. Notwithstanding, after sputtering the LEIS spectrum gives a pure W peak, and the contaminants are not completely extracted: in fact, sputter cleaning removes solely the contaminants of the outermost layer(s).

The high-temperature heating of the specimens restores their sputter-induced surface chaos and stimulates the C migration out of the undersurface location to the outermost layer. An optimal way of a C extraction from the outermost layer, together with the C depletion from an undersurface location, consists in heating the W specimens in  $\text{O}_2$  gas. As a rule, the C depletion is made in a separate chamber by annealing the specimens with EB at 1500 K in  $\text{O}_2$  gas ( $10^{-5}$  mbar). A release of C from the outermost layer stimulates the further traveling of C to the surface, which is afterward released by vacuum extraction of CO. At the final steps, the specimens have been flashed in UHV at 2500 K to extract O from the surface. C and O remaining after this procedure are removed by repeated cleaning. As a result of the C migration from the volume to the surface layers at the initial steps, a superstructure on the W(1 1 0) specimen forms, which is shown in **Figure 5**. After continued treatment the surface region is completely free of C, and alone O is present on the W surface after annealing in  $\text{O}_2$ . So, no more C migrates to the surface of the specimens when the surplus O is extracted by flashing.

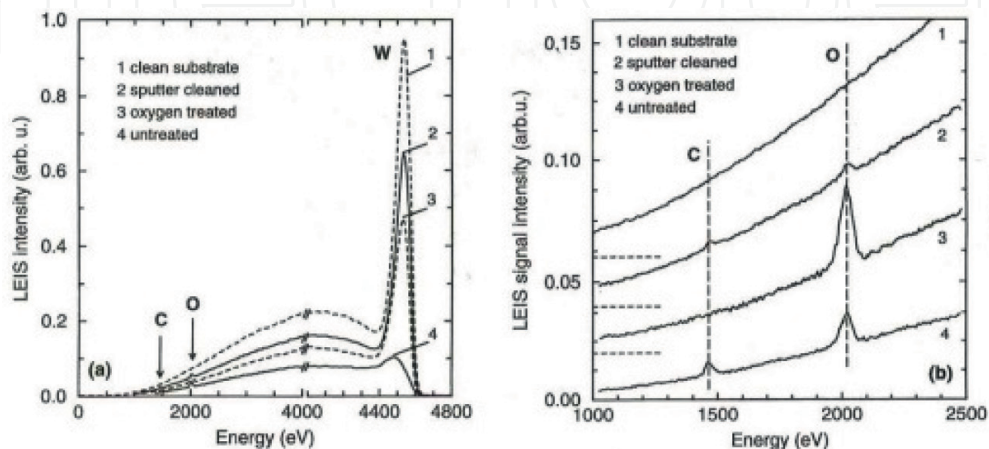


**Figure 3.** LEIS 5 keV  $\text{He}^+$  spectra obtained after different cleaning steps of the W(1 1 0) specimens: (a) complete spectra and (b) energy range covering only the C and O peaks. The baselines of the spectra in (b) are indicated by the dashed lines. The AES spectra if the corresponding stages are shown in **Figure 4**.



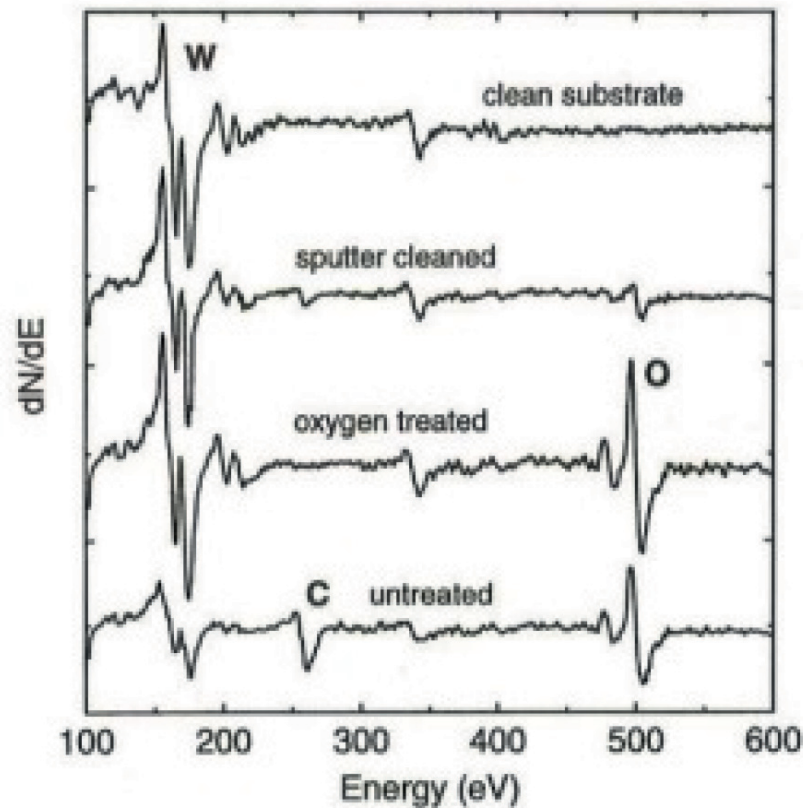


**Figure 4.** The AES spectra at the different cleaning stages of the  $W(1\ 1\ 0)$  specimens. The LEIS spectra of the corresponding stages are shown in Figure 3.

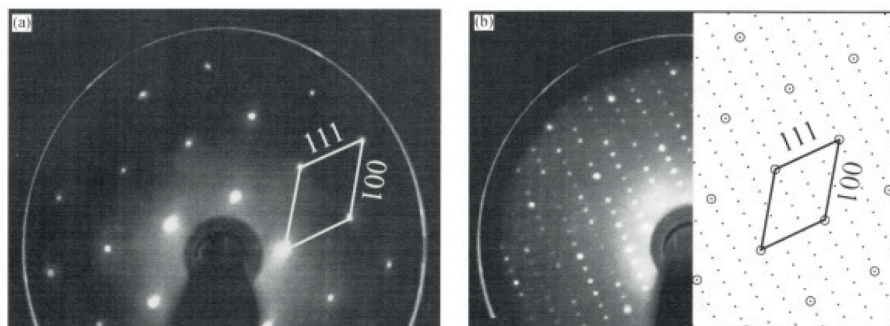


**Figure 5.** LEED patterns of the  $W(1\ 1\ 0)$  specimens at an energy of 300 eV: (a) clean unreconstructed  $W(1\ 1\ 0)$  and (b) C superstructure after flashing in initial cleaning.

## 2.4 Tensile samples

Tensile specimens are produced by a step-by-step treatment. At first, to get small rods with 1.6 mm in diameter and 27 mm in length, large AG crystals are cut [8–12]. Small rods are processed by a round hollow electrode to decrease in diameter of a gauge part. After processing, the specimens of 1.3 mm in diameter and of 14 mm in length are produced, with shoulders of 1.6 mm in diameter on both ends. Then, the specimens are chemically polished to move away a damaged layer of 0.05 mm. Then, the specimens are suspended in the center of the hollow electrode. Both the electrode and specimen are put into 1% NaOH which flows through the hollow electrode along the specimen. When an electric current is on, the diameter of a specimen is decreased by etching to its final sizes of 0.9 mm and free from of

0.15 mm of a damaged layer. Such controllable simple step-by-step treatment allows to get a constant diameter along the gauge part. The tensile specimens are plastically deformed at a constant strain rate of  $8.5 \times 10^{-4} \text{ s}^{-1}$  on two deformation setups with different  $T$ . Below, 320 K tests are done in a He cryostat which is fixed on an Instron. Type-A tests consist in isothermal plastic deformation of several samples to their ultimate tensile strain at different  $T$ . Type-B tests represent successive deformation in a little strain interspace at different  $T$  after a first deformation at  $>600 \text{ K}$ .

## 2.5 Experimental results

In **Figure 6**, the shear stress  $\tau$  is depended on the shear strain  $\epsilon_p$  for samples deformed to neck formation or fracture at constant  $T$ . Parabolicity of the curves below 400 K in **Figure 6** connects with severe hardening at little  $\epsilon_p$ . At  $T = 650 \text{ K}$ , a slight hardening is seen up to  $\epsilon_p \leq 0.04$ ; however, at  $\epsilon_p \geq 0.04$ , constant values of shear stresses are observed.

In spite of that, tensile specimens are produced with a great care; some of them can only be deformed to little  $\epsilon_p$ , more pronounced at the lowest  $T$ . For  $\epsilon_p = 0.001$ , the hardening rates increase more with lowering  $T$ , for example, to 70,000 MPa at 26 K. For  $\epsilon_p \geq 0.01$ , the hardening rates are less at low  $T$  and a dependence of  $T$  lowers faster. In turn, parabolicity of the hardening curves prevents determining the critical shear stress. It is interesting that any problems do not appear if the specimens are subjected to small deformation at decreasing  $T$  after the prime

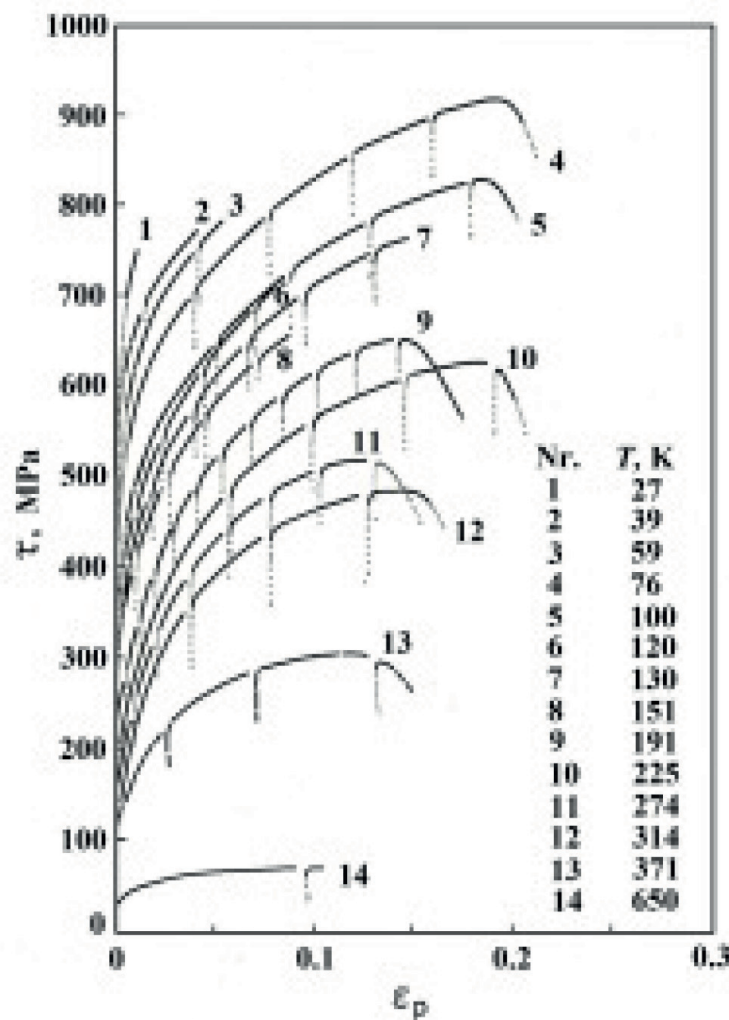


**Figure 6.**  
 Tests (A): shear stress  $\tau$  versus shear strain  $\epsilon_p$  of W at different  $T$ .

deformation to  $\varepsilon_p \approx 0.08$  at  $T > 600$  K (B-tests). **Figure 7** shows such curves received for one specimen for the shear stress  $\tau$  as a function of the shear strain  $\varepsilon_p$ . It is important to note that at the prime deformation at 621 K after a short hardening regime, the stress has reached a *plateau*. However, subsequent plastic deformation at 586 and 541 K is not accompanied by hardening. At lower temperatures, the phenomenon of transition to the yield point (186 and 151 K) occurs.

In **Figure 8**, all experimental data of our tests are shown. The shear stresses, corresponding to the plateau and the lower yield stresses, are referred as a critical shear stress  $\tau_c$ . They are plotted against  $T$  in the range of 50–800 K (**Figure 8**). The results of tensile tests in various cooling or heating conditions match in the best way [8–12]. Above 740 K, with increasing  $T$ ,  $\tau$  changes very little. The critical shear stress  $\tau_c$  at 800 K is not high ( $\tau \approx 13$  MPa), which is consistent with both the high purity and structural quality of tested W specimens. The value of  $\tau$  down to low  $T$  increases very fast and parabolically. At 600–620 K, a pronounced transition to a semi-linear increase in  $\tau$  is seen at lowering  $T$  to 200–250 K. Then, a plain transition to a solid rise in  $\tau$  with lowering  $T$  can be seen. In accordance with this form of  $\tau(T)$ , it can be summarized that W single crystals of high-purity exhibit a three-stage

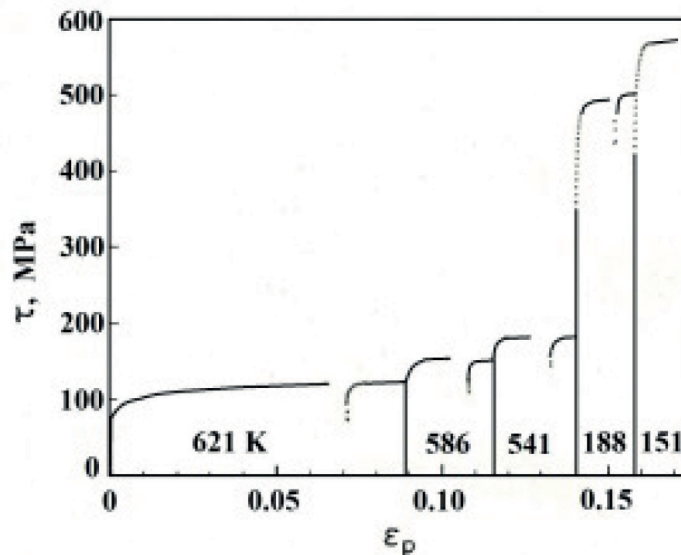


**Figure 7.**  
B-tests: successive deformations of one W specimen at decreasing  $T$ .

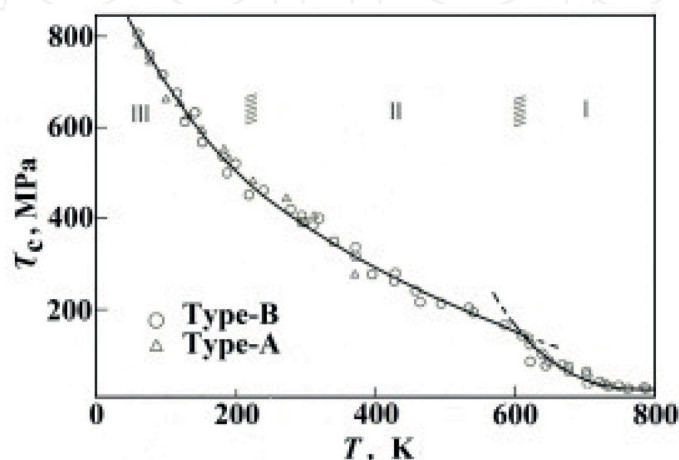


**Figure 8.**  
The temperature dependence of  $\tau_c$  for B-tests (A-tests also involved).

mechanical behavior (I, II, and III). This is also characteristic of plasticity of other BCC metals like Mo or Nb [13–17].

### 3. Conclusions

1. The estimates show that the axial gradients of  $T$  under the crystallization front in the solid phase can reach  $1500 \text{ K cm}^{-1}$ . This leads to significant thermal stresses followed by their relaxation through plastic flow and multiplication of dislocations. In other words, the temperature gradients cause high values of the dislocation density, which leads to the appearance of a characteristic dislocation substructure. In the crystals with the growth axis  $[1\ 0\ 0]$ , there are small-angle boundaries elongated along the growth axis and having misorientations up to  $1\text{--}2^\circ$ . A fairly high ratio of the resistances of the investigated single crystals of W at the level of  $\sim 10^4$  to  $10^6$  indicates a high purity of the metal, which leads to an unambiguous conclusion about the insignificant role of impurities in the development of the crystal dislocation structure.
2. W single crystals oriented for single slip have been tested in dynamical tensile tests between 26 and 800 K. The critical shear stress  $\tau_c$  at 800 K is not high ( $\tau \approx 13 \text{ MPa}$ ), which is consistent with both the high purity and structural quality of tested W specimens. The value of  $\tau$  down to low  $T$  increases very fast and parabolically. Qualitatively, these results agree well with type-A and type-B tests with high-purity Mo single crystals. The measurements confirm also for the W single crystals the existence of three regimes of the dependence of the flow stress on temperature which results meet quite well with known results of other BCC metals studied.


IntechOpen

#### Author details

Vadim Glebovsky  
Institute of Solid State Physics, The Russian Academy of Sciences, Chernogolovka,  
Russia

\*Address all correspondence to: [glebovs@issp.ac.ru](mailto:glebovs@issp.ac.ru)

#### IntechOpen

© 2018 The Author(s). Licensee IntechOpen. This chapter is distributed under the terms of the Creative Commons Attribution License (<http://creativecommons.org/licenses/by/3.0>), which permits unrestricted use, distribution, and reproduction in any medium, provided the original work is properly cited. 



## References

- [1] Lassner E, Schubert WD, editors. Tungsten: Properties, Chemistry, Technology of the Element, Alloys and Chemical Compounds. New York: Kluwer Academic/Plenum Publishers; 1998
- [2] Chaika A, Orlova N, Semenov V, Postnova E, Krasnikov S, Lazarev M, et al. Fabrication of [001]-oriented tungsten tips for high resolution scanning tunneling microscopy. Scientific Reports. 2014;**4**:3742
- [3] Glebovsky V. Highly pure refractory metals for thin film metallization of VLSI. Chapter 13. In: Ho Yeap K, editor. Very-Large-Scale Integration. Rijeka: InTech; 2018. pp. 67-109. ISBN: 978-953-51-5309-2. DOI: 10.5772/intechopen.69126
- [4] Cortenraad R, Ermolov S, Semenov V, Denier van der Gon A, Glebovsky V, Bozhko S, et al. Growth, characterization and surface cleaning procedures for high-purity tungsten single crystals. Journal of Crystal Growth. 2001;**222**:154-162
- [5] Bozhko S, Glebovsky V, Semenov V, Smirnova I. Study on the growth of tungsten single crystals of high structural quality. Journal of Crystal Growth. 2008;**311**:1-6. DOI: 10.1063/1.3254240
- [6] Glebovsky V. In: Sztwiertnia K, editor. Crystal Growth: Substructure and Recrystallization. Rijeka: InTech; 2012. pp. 59-86
- [7] Cortenraad R, Ermolov S, Semenov V, Denier van der Gon A, Glebovsky V, Bozhko S, et al. Electron-beam growing and purification of W crystals. Vacuum. 2001;**62**:181-188
- [8] Brunner D, Diehl J, Glebovsky V. The plastic behavior of high-purity tungsten. In: Proceedings of the 5th International Conference on Ultra High-Purity Materials (UHPM-98); Sevrier, Annecy Lake, France; 1998. pp. 83-92
- [9] Brunner D, Glebovsky V. The plastic properties of high-purity W single crystals. Materials Letters. 2000;**44**:144-152
- [10] Brunner D, Glebovsky V. Analysis of flow-stress measurements of high-purity W single crystals. Materials Letters. 2000;**44**:290-296
- [11] Brunner D. Comparison of flow-stress measurements on high-purity tungsten single crystals with the kink-pair theory. Materials Transactions of Japan Institute of Metals. 2000;**41**:152-160
- [12] Brunner D. Peculiarities of work-hardening of high-purity tungsten single crystals below 800 K. Materials Science and Engineering A. 2004;**387**:167-170
- [13] Hull D, Beardmore P, Valentine A. Crack propagation in single crystals of tungsten. Philosophical Magazine. 1965;**12**:1021-1041
- [14] Butler B, Paramore J, Ligda J, Ren C, Fang Z, Middlemas S, et al. Mechanisms of deformation and ductility in tungsten—A review. International Journal of Refractory Metals and Hard Materials. 2018;**75**:248-261. DOI: 10.1016/j.ijrmhm.2018.04.021
- [15] Wang J, Zeng Z, Weinberg C, Zhang Z, Zhu T, Mao S. *In situ* atomic scale observation of twinning-dominated deformation in nanoscale body-centred cubic tungsten. Nature Materials. 2015;**14**(6):594-600. DOI: 10.1038/NMAT4228
- [16] Liu G, Song, Liu M, X, Ni S, Wang S, He Y, Liu Y. An investigation of the

mechanical behaviors of micro-sized tungsten whiskers using nanoindentation. *Materials Science and Engineering A*. 2014;**594**:278-286. DOI: 10.1016/j.msea.2013.11.084

[17] Riedle J, Fischmeister H, Gumbsch P, Glebovsky V, Semenov V. Fracture studies of tungsten single crystals. *Materials Letters*. 1994;**20**:311-320

IntechOpen

IntechOpen